molecules

MDPI

Communication

On the Photostability of Cyanuric Acid and Its Candidature as a Prebiotic Nucleobase

Luis A. Ortiz-Rodríguez *, Sean J. Hoehn and Carlos E. Crespo-Hernández *

Department of Chemistry, Case Western Reserve University, Cleveland, OH 44106, USA; sxh905@case.edu
* Correspondence: lao21@case.edu (L.A.O.-R.); carlos.crespo@case.edu (C.E.C.-H.)

Abstract: Cyanuric acid is a triazine derivative that has been identified from reactions performed under prebiotic conditions and has been proposed as a prospective precursor of ancestral RNA. For cyanuric acid to have played a key role during the prebiotic era, it would have needed to survive the harsh electromagnetic radiation conditions reaching the Earth's surface during prebiotic times (≥200 nm). Therefore, the photostability of cyanuric acid would have been crucial for its accumulation during the prebiotic era. To evaluate the putative photostability of cyanuric acid in water, in this contribution, we employed density functional theory (DFT) and its time-dependent variant (TD-DFT) including implicit and explicit solvent effects. The calculations predict that cyanuric acid has an absorption maximum at ca. 160 nm (7.73 eV), with the lowest-energy absorption band extending to ca. 200 nm in an aqueous solution and exhibiting negligible absorption at longer wavelengths. Excitation of cyanuric acid at 160 nm or longer wavelengths leads to the population of $S_{5,6}$ singlet states, which have ππ* character and large oscillator strengths (0.8). The population reaching the $S_{5,6}$ states is expected to internally convert to the $S_{1,2}$ states in an ultrafast time scale. The $S_{1,2}$ states, which have nπ* character, are predicted to access a conical intersection with the ground state in a nearly barrierless fashion (ca. ≤ 0.13 eV), thus efficiently returning the population to the ground state. Furthermore, based on calculated spin–orbit coupling elements of ca. 6 to 8 cm^{-1}, the calculations predict that intersystem crossing to the triplet manifold should play a minor role in the electronic relaxation of cyanuric acid. We have also calculated the vertical ionization energy of cyanuric acid at 8.2 eV, which predicts that direct one-photon photoionization of cyanuric acid should occur at ca. 150 nm. Collectively, the quantum-chemical calculations predict that cyanuric acid would have been highly photostable under the solar radiation conditions reaching the Earth's surface during the prebiotic era in an aqueous solution. Of relevance to the chemical origin of life and RNA-first theories, these observations lend support to the idea that cyanuric acid could have accumulated in large quantities during the prebiotic era and thus strengthens its candidature as a relevant prebiotic nucleobase.

Keywords: cyanuric acid; prebiotic era; photostability; RNA ancestors; excited-state calculations

Citation: Ortiz-Rodríguez, L.A.; Hoehn, S.J.; Crespo-Hernández, C.E. On the Photostability of Cyanuric Acid and its Candidature as a Prebiotic Nucleobase. *Molecules* **2022**, *27*, x. https://doi.org/10.3390/xxxxx

Academic Editor(s): Tolga Karsili and Barbara Marchetti

Received: 19 December 2021
Accepted: 05 February 2022
Published: date

1. Introduction

The origin and prebiotic ancestral lineage of ribonucleic acid (RNA) has been a mystery captivating scientists from all research backgrounds for many years. A principal focus of the RNA-world hypothesis surrounds the probiotic synthesis of RNA and its plausible precursors. Several triazine derivatives have been identified from reactions performed under prebiotic conditions as well as in meteorites, making their formation and existence in early Earth as precursors highly probable [1,2] Specifically, melamine, ammeline, ammelide and cyanuric acid (CA) have been identified to spontaneously form from a simple gas mixture of CO, H_2 and NH_3 [3,4]. Recently, Jeilani et al. proposed free radical-mediated mechanisms that lead to the formation of the triazine derivatives, melamine, ammeline, ammelide and CA based on density functional theory calculations (DFT)

that are reasonable for prebiotic scenarios [5]. Their results showed that CA has the shortest mechanism for formation and that the keto-tautomer should be the most stable [5].

CA is the triazine derivative of barbituric acid (BA), which has been proposed as a prebiotic ancestor of canonical RNA [6,7]. Interestingly, CA was found to spontaneously self-assemble to form a stable cyclic hexamer [8] Additionally, CA has been identified to form supramolecular structures when hydrogen bonded to 2,4,6-triaminopyrimidine (TAP), which has been proposed as a promising prebiotic ancestor of the RNA nucleobases [6,7] The standard-state free energy of CA incorporated into the higher ordered polymers was found to be −3.3 kcal/mol, which corresponds well with the standard free energy between canonical nucleobases within folded RNA structures [9,10]. Furthermore, Karunakaran et al. investigated polymer formation of TAP modified with a hexanoic acid tail [11] While individually these monomers are achiral, upon polymerization the superhelical structures were identified through circular dichroism to have alternating domains of chirality within the same sample. However, when the CA derivative was provided as mainly a specific enantiomer for the polymer formation, homopolymer superhelical structures resulted, similar to what was observed in duplex DNA [11]. This result, along with the structural similarity of CA: TAP, CA: melamine, and the typical Watson–Crick base pairing observed in the canonical nucleobases, supports the idea that CA could be a plausible prebiotic ancestor of RNA.

Importantly, however, for CA to have played an important role during the prebiotic era on Earth, it would have needed to survive the extreme conditions of those times to accumulate in significant amounts. Of particular relevance to this investigation, protection against UV radiation would have likely been an important selection criterion [12] During the early Earth, the environmental conditions were much different than those present today, including the absence of an atmospheric ozone layer. However, atmospheric gases such as water and CO_2 attenuated high energy radiation below 6.2 eV (200 nm) [13,14] Therefore, even though it has been shown that CA can be formed under both prebiotic and astrophysical conditions, its photophysical and photochemical properties should be studied to predict its potential availability and participation in prebiotic chemistry.

In this study, we investigated the photostability likelihood of CA using DFT and its time-dependent variant (TD-DFT). The earliest time that life forms first appeared on Earth was around 4 billion years ago [15–17] and a recent study estimated the pH to be 6.6 [18] around that time. Therefore, we focus solely on the tri-keto tautomer of CA in this investigation because the pK_a of CA is 6.9 [9]. It is predicted that CA has minimal absorption at longer wavelengths than 200 nm, in agreement with the incomplete experimental data available for CA [19] Furthermore, the calculations predict that excitation of the optically bright $S_{5,6}(\pi\pi^*)$ states should lead to ultrafast internal conversion to the ground-state through $^1n\pi^*/S_0$ conical intersections, which—taken together with the calculation of relatively small singlet-triplet spin–orbit couplings—suggest that a significant population of long-lived reactive triplet states is unlikely.

2. Results and Discussion

2.1. Ground-State Structure and Absorption Spectrum of CA

Figure 1 shows the optimized ground-state structure of neutral tri-keto CA microsolvated with three explicit water molecules forming hydrogen bonds with the hydrogen and oxygen atoms at the X3LYP/C-PCM/cc-pVDZ level of theory in water. The X3LYP is a double-hybrid functional based on the Lee–Yang–Parr correlation functional designed to improve the accuracy of nonbonded interactions such as hydrogen bonds [20,21]. As shown in Figure 1, the bond lengths between nitrogen–carbon and carbon–oxygen are 1.38 and 1.23, respectively, regardless of the bond examined and not surprisingly since the molecule has D_3h symmetry.

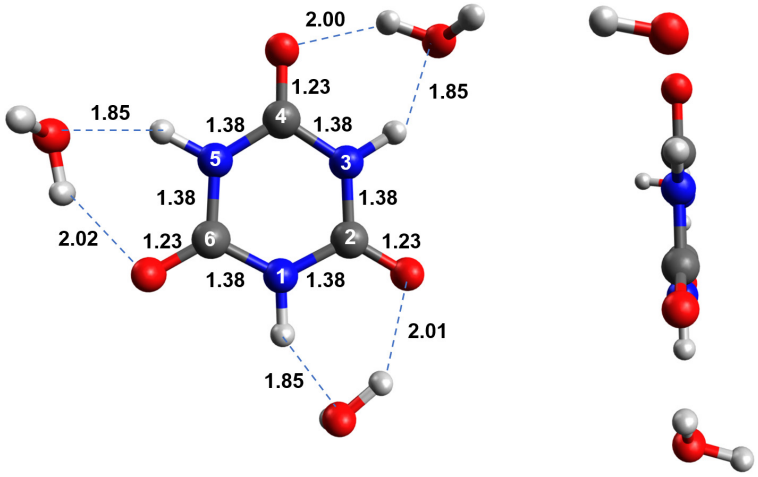

Figure 1. Optimized ground-state structure of neutral tri-keto CA microsolvated with three water molecules at the X3LYP/C-PCM/cc-pVDZ level of theory in water. Standard atom numbering is shown in white, while relevant bond lengths (in angstroms) are shown in black.

Vertical excitation energies for the first six excited singlet states of microsolvated CA are reported in Table 1 at the TD-CAM-B3LYP/C-PCM/def2-TZVP//X3LYP/C-PCM/cc-pVDZ level of theory in water. In addition to the range-separated hybrid functional, CAM-B3LYP, [22] two other range-separated hybrid functionals, ωB97X [23] and LC-PBE, [24] and the hybrid functional, PBE0 [25], were evaluated to calculate the vertical excitation energies to compare their performance. The vertical excitation energies obtained with the range-separated hybrid functionals (i.e., CAM-B3LYP, ωB97X and LC-PBE) are within the mean standard deviation error (0.2–0.3 eV) of vertical excitation energies obtained with electronic-structure methods [26,27] and thus, from this point forward, and for simplicity, we focus in the main text on the results obtained with the CAM-B3LYP functional. The vertical excitation energies for the first six excited singlet states of microsolvated CA with ωB97X and LC-PBE functionals are reported in Table S1, whereas the results obtained with the PBE0 functional are reported in Figure S1 and Tables S2 and S3.

Table 1. Vertical excitation energies for the lowest six singlet and nine triplet states of microsolvated CA calculated at the TD-CAM-B3LYP/C-PCM/def2-TZVP//X3LYP/C-PCM/cc-pVDZ in water. States expected to play a plausible role in the electronic relaxation mechanism are highlighted in bold.

State	Character	Energy (eV)
S_1	**$n\pi^*$**	**6.34 (0.000)**
S_2	**$n\pi^*$**	**6.34 (0.000)**
S_3	$\pi\pi^*$	6.86 (0.000)
S_4	$\pi\pi^*$	6.91 (0.000)
S_5	**$\pi\pi^*$**	**7.73 (0.80)**
S_6	**$\pi\pi^*$**	**7.73 (0.80)**
T_1	**$\pi\pi^*$**	**5.74**
T_2	**$\pi\pi^*$**	**5.74**
T_3	$n\pi^*$	5.76
T_4	$n\pi^*$	5.76
T_5	**$\pi\pi^*$**	**5.81**
T_6	$n\pi^*$	6.32
T_7	$\pi\pi^*$	6.49
T_8	$\pi\pi^*$	6.69
T_9	$\pi\pi^*$	6.70

As shown in Table 1, there are states with equal energy, character, and oscillator strength due to the high symmetry of the molecule (D_3h). Based on the oscillator strengths of the transitions, only the $S_5(\pi\pi^*)$ and $S_6(\pi\pi^*)$ excited singlet states have a significant contribution to the absorption spectrum of CA in water. Hence, only these two states were considered in the calculated absorption spectrum of microsolvated CA reported in Figure 2. To generate the absorption spectrum, each transition was convoluted with a Gaussian function (FWHM = 16 nm). The absorption spectrum should be a result of the linear combination of the individual Gaussian functions of each transition, which resulted in a Gaussian band with FWHM = 28 nm. Since both states have the same vertical energy and oscillator strength, the same result is obtained by multiplying the Gaussian function of one of the states by two. This calculated absorption spectrum agrees with the absorption tail reported by Sancier et al. for CA at pH 4.4. [19] The use of Gaussian functions with FWHM < 16 nm to convolute the individual transitions was also attempted but did not accurately describe the absorption tail reported by Sancier et al. [19] Furthermore, the FWHMs of the fully-resolved lowest-energy absorption band reported by Sancier et al. [19] for CA at pH 9.7 (i.e., for deprotonated CA) and that of the similar compound TAP [6] at pH 7.4 are ~25 nm. Therefore, we consider the methodology used herein to model the lowest-energy absorption band of neutral CA to be reasonable. Accordingly, as shown in Figure 2, CA has an absorption maximum at 160 nm and has a tail that extends to ca. 205 nm based on our modeling of the lowest-energy absorption band. Notably, the absorption coefficients above 200 nm are small (<1.5 × 10^3 M^{-1} cm^{-1}) and a comparatively small absorption is expected if CA is irradiated at longer wavelengths than 200 nm.

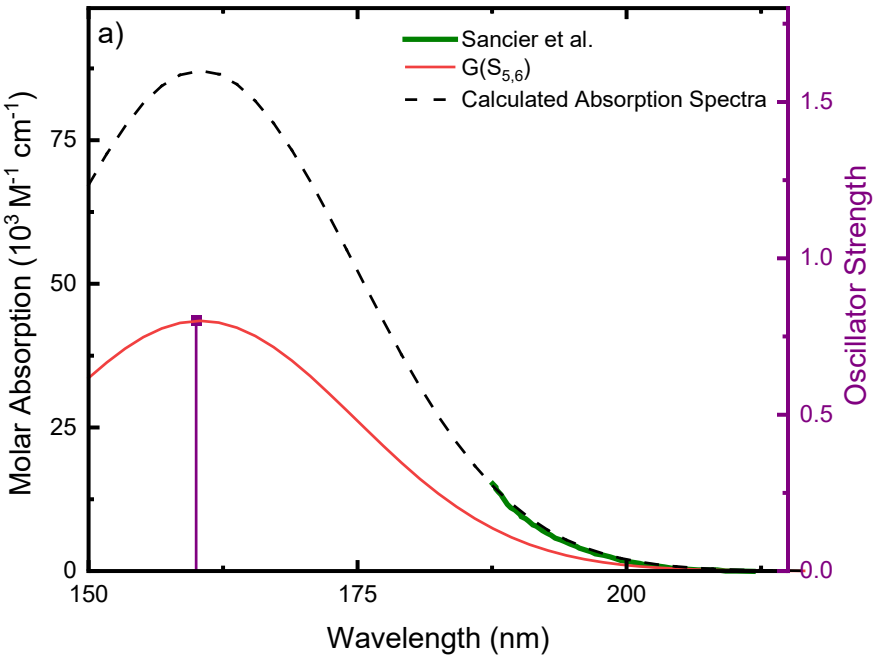

Figure 2. Calculated ground-state absorption spectrum of microsolvated CA at the TD-CAM-B3LYP/C-PCM/def2-TZVP//X3LYP/C-PCM/cc-pVDZ in water. The S_5 and S_6 oscillator strengths were convoluted with a Gaussian function (FWHM = 16 nm) centered at the vertical excitation energy of each state. The calculated absorption spectrum (dashed black line) is the result of the sum of the individual Gaussian functions of each state (red). Since both states have the same vertical energy and oscillator strength, the same result is obtained by multiplying the Gaussian function of one of the states by two. Shown in green is the absorption tail of CA at pH 4.4 [19].

2.2. Plausible Photochemical Deactivation Pathways of CA in Water

Vertical excitation energies were calculated for microsolvated CA at the TD-CAM-B3LYP/C-PCM/def2-TZVP//X3LYP/C-PCM/cc-pVDZ level of theory in water (Table 1) to

estimate the absorption spectrum (vide supra) of CA, but also to characterize the ordering of the states in the Franck–Condon region and to propose plausible electronic transitions for intersystem crossing to the triplet manifold. Hence, the vertical excitation energies for excited triplet states that are isoenergetic or lower in energy than the $S_{5,6}(\pi\pi^*)$ states are also reported in Table 1. We considered excited states equal or lower in energy than the $S_{5,6}(\pi\pi^*)$ state because, as shown in Figure 2, if CA were to absorb radiation around its absorption maximum of ca. 160 nm, the $S_{5,6}(\pi\pi^*)$ states would be the primary electronic states to be populated. Note that the S_4 to S_1 states are predicted to have negligible oscillator strengths (independent of their electronic character) according to the calculations, and, hence, should not be populated upon direct absorption of electromagnetic radiation. We also remark that the character of the excited states reported in Table 1 is based on the inspection of the primary one-electron transition Kohn–Sham orbitals for each electronic state.

Based on El-Sayed's propensity rules, [28,29] and assuming that the population reaching the $S_{5,6}(\pi\pi^*)$ states will internally convert to the $S_{1,2}(\pi\pi^*)$ states in an ultrafast time scale (i.e., obeying the Kasha's rule), [30] the $S_{1,2} \rightarrow T_5$ and $S_{1,2} \rightarrow T_{1,2}$ electronic transitions could in principle compete with internal conversion from the $S_{1,2}(\pi\pi^*)$ states (i.e., by radiative and/or nonradiative processes) to the ground state. Hence, to further evaluate the probability of intersystem crossing pathways, the spin–orbit couplings between these transitions are reported in Table 2 for microsolvated CA at the TD-CAM-B3LYP/C-PCM/def2-TZVP//X3LYP/C-PCM/cc-pVDZ level of theory in water. We note that the magnitude of the spin–orbit coupling elements between other singlet–triplet excited state combinations presented in Table 1 with energy gaps lower than 0.5 eV are significantly smaller (ca. < 0.1 cm^{-1}) than those shown in Table 2 (not shown). As displayed in Table 2, the magnitudes of the spin–orbit couplings are small (ca. 6 to 8 cm^{-1}) but not necessarily negligible and may contribute to a very low yield of triplet state population. We note that the magnitude of the spin–orbit couplings predicted herein for CA are within the same order of magnitude as those reported for TAP (5 to 10 cm^{-1}), [31] which has been shown by Brister et al. [6] to be highly photostable due to ultrafast fast relaxation pathways leading to a ground state in an aqueous solution. In addition, Rankine [31] located five different S_1/S_0 minimum-energy crossing points (MECP) for TAP in agreement with the ultrafast deactivation and photostability reported by Brister et al. [6]. Furthermore, the molecular structure of CA resembles that of uracil, but with a carbon atom replacing the N5 atom and the addition of a carbonyl at the C6 position. Uracil monomers are photostable due to the availability of accessible conical intersections between the excited singlet states and the ground state, [32–37] and they populate the triplet state with less than ca. 1% yield in an aqueous solution [38]. Thus, considering the body of work reported for TAP and for the uracil monomers, we propose that triplet state population in CA should be very small (if not insignificant) in water.

Table 2. Energy gaps between the calculated excited singlet and triplet states and their corresponding spin–orbit couplings obtained for microsolvated CA at the TD-CAM-B3LYP/C-PCM/def2-TZVP//X3LYP/C-PCM/cc-pVDZ level of theory in water. [a]

Transition	ΔE (eV)	SOCs (cm^{-1})
$S_{1,2}T_{1,2}$	0.48	6.3
$S_{1,2}T_5$	0.36	8.0

[a] assuming ultrafast internal conversion from the $S_{5,6}(\pi\pi^*)$ to the $S_{1,2}(\pi\pi^*)$ states.

To further support this idea, we decided to investigate the availability of conical intersections between the S_1 and S_0 states in CA, which—together with the results reported above—should provide a more complete picture of the primary relaxation mechanism. Figure 3 shows the S_1 minimum and the geometry of a conical intersection ($(S_1/S_0)_{CI}$) that were optimized with the linear response implementation of TD-DFT (LR-TD-DFT). The $(S_1/S_0)_{CI}$ exhibits C-puckering and significant out of plane displacement of the oxygen

atom. Hereafter, we will label the puckering as C6-puckering for simplicity (i.e., the carbon atom that is puckered corresponds to the carbon atom that was labeled as C6 in Figure 1. However, due to the symmetry of CA, this C-puckering also applies to the C2 and C4 atoms. To obtain an estimation of a putative energy barrier to access the conical intersection, we performed optimizations along the O6C6N1C2 dihedral angle to capture the C6 puckering and the out of plane displacement of the oxygen atom going from the S_1 minimum-geometry to the $(S_1/S_0)_{CI}$. The potential energy profiles are reported in Figure 4. As shown in Figure 4, the calculations predict that the $(S_1/S_0)_{CI}$ can be accessed in a nearly barrierless (0.03 eV) fashion, which suggests that this conical intersection could play a major role in the deactivation of CA. Therefore, these results, together with the spin–orbit couplings reported above, suggest that CA should be highly photostable following photoactivation.

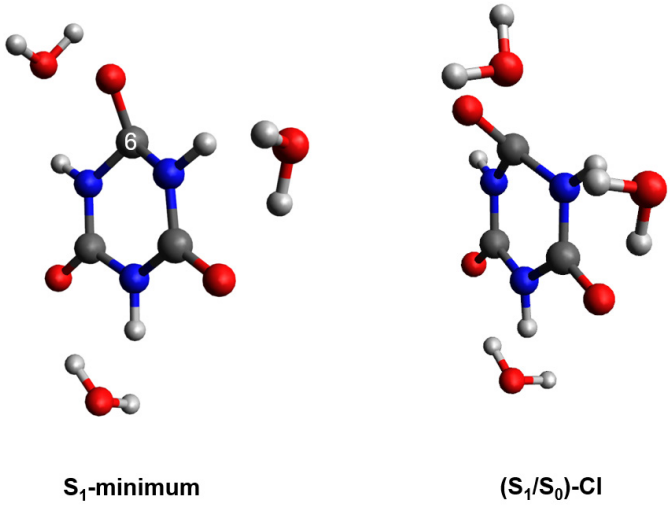

Figure 3. Optimized S_1 minimum-geometry and the $(S_1/S_0)_{CI}$ along the C6-puckering coordinate obtained for microsolvated CA at the TD-X3LYP/C-PCM/cc-pVDZ in water.

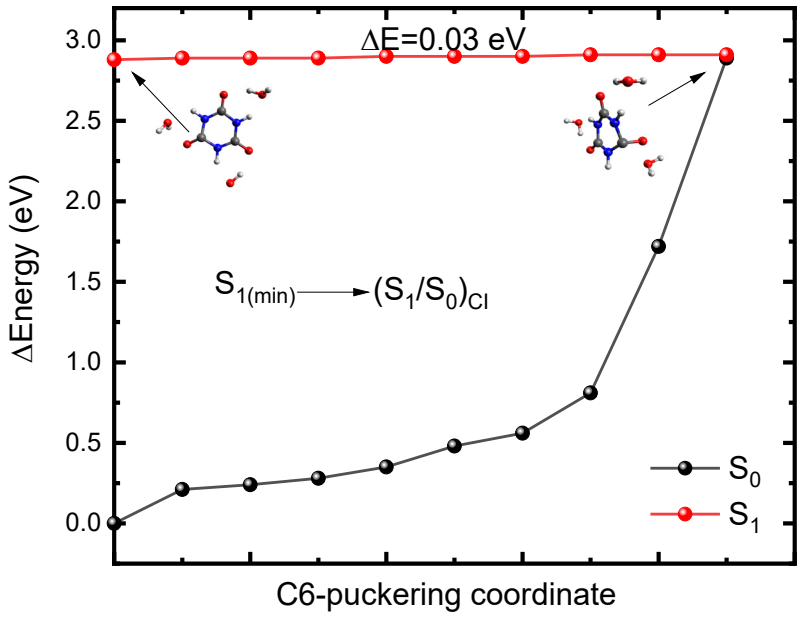

Figure 4. Potential energy profiles between the S_1 minimum-geometry and the $(S_1/S_0)_{CI}$ along the C6-puckering coordinate obtained for microsolvated CA at the TD-CAM-B3LYP/C-PCM/def2-

TZVP//X3LYP/C-PCM/cc-pVDZ in water. Inset: Molecular structure of the S_1 minimum-geometry and the $(S_1/S_0)_{CI}$. ΔE represents the energy barrier to access the conical intersection.

At this point, it is important to highlight that we are aware of the limitations of linear response (LR) TD-DFT in predicting the correct dimensionality of conical intersections between the ground and excited states due the single-reference nature of this method [39]. Therefore, to further strengthen the idea of the availability of a $(S_1/S_0)_{CI}$, we decided to employ the spin–flip (SF) approach of TD-DFT (SF-TD-DFT) [40,41]. The SF approach has been used extensively to overcome the problem with the conical intersections between the ground and excited states [40–42]. In SF-TD-DFT, the idea is to use a different reference for the state of interest. For instance, in SF-TD-DFT, the singlet states are generated via excitation from a triplet reference state. Several studies have shown the correct dimensionality of the conical intersections obtained with SF-TD-DFT [40,43,44]. Thus, we assume that this methodology should provide a qualitatively correct picture of the system. Figure 5 shows the S_1 minimum and the geometry of a conical intersection ($(S_1/S_0)_{CI}$) that was optimized with SF-TD-DFT. As the $(S_1/S_0)_{CI}$ found with LR-DT-DFT, this conical intersection exhibits C-puckering and significant out of plane displacement of the oxygen atom. However, the C-puckering and the displacement of the oxygen atom are more pronounced in the $(S_1/S_0)_{CI}$ obtained with SF-TD-DFT. As shown in Figure 6, the $(S_1/S_0)_{CI}$ can be accessed from the S_1 minimum by overcoming a small energy barrier (0.13 eV). We note that this energy barrier is only 0.1 eV higher than the energy barrier found when LR-TD-DFT is used to find the $(S_1/S_0)_{CI}$. Thus, the qualitative agreement between the LR-TD-DFT and SF-TD-DFT results, together with the vast body of work that has reported analogous conical intersections for similar molecules [32–37] strengthen the idea of the prospective availability of S_1/S_0 conical intersections and, as discussed above, the high photostability of this system. However, acknowledging the limitations of the methodology employed herein, we hope that these calculations will motivate theoretical groups that employ multireference methodologies to not only examine the availability of S_1/S_0 conical intersections such as the one reported here, but to also investigate whether the higher lying $S_{5,6}(\pi\pi^*)$ states have access to conical intersections with the S_1 or the S_0 state out of the Franck–Condon region.

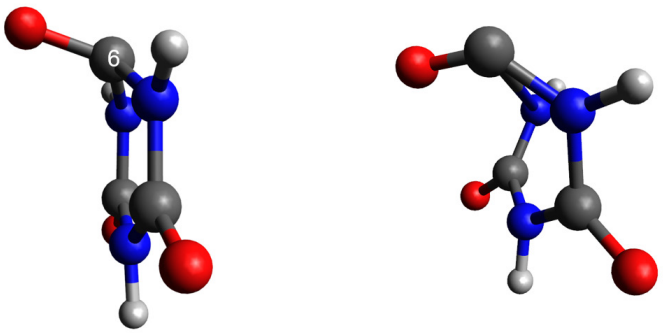

Figure 5. Optimized S_1 minimum-geometry and the $(S_1/S_0)_{CI}$ found using SF-TD-DFT along the C6-puckering coordinate obtained for CA at the TD-X3LYP/C-PCM/cc-pVDZ in water.

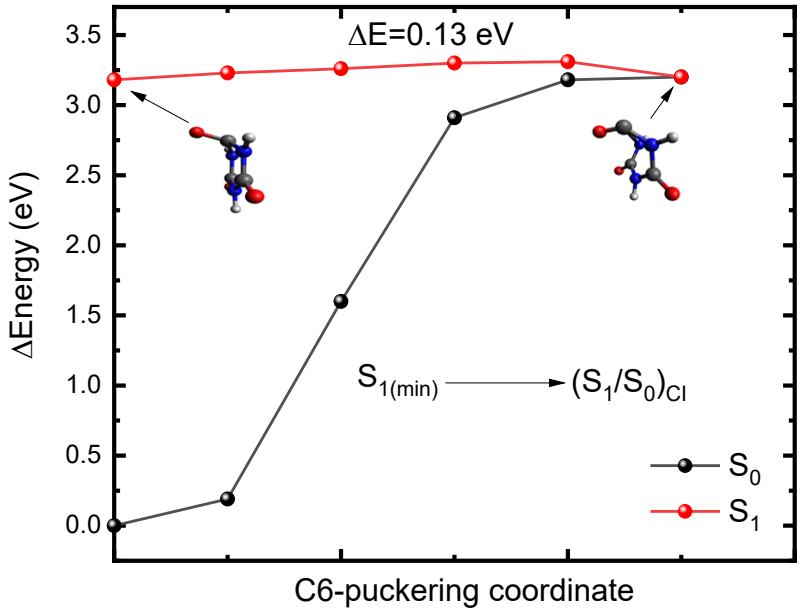

Figure 6. Potential energy profiles based on the minimum-energy paths between the S_1 minimum-geometry and the $(S_1/S_0)_{CI}$ found using SF-TD-DFT along the C6-puckering coordinate obtained for CA at the TD-X3LYP/C-PCM/cc-pVDZ in water. Inset: Molecular structure of the S_1 minimum-geometry and the $(S_1/S_0)_{CI}$. ΔE represents the energy barrier to access the conical intersection.

Finally, another photochemical pathway that should be considered is direct photoionization of CA, which can lead to the formation of reactive radicals and the eventual degradation of CA. To evaluate this possibility, we calculated the vertical ionization energy of microsolvated CA in water at the UX3LYP/C-PCM/cc-pVDZ level of theory. The predicted vertical ionization energy is equal to 8.2 eV (151 nm), or 791.2 kJ/mol (189.1 kcal/mol). Therefore, given that atmospheric gases such as water and CO_2 attenuated high energy radiation at shorter wavelengths than 200 nm on the prebiotic Earth's surface, the calculations predict that direct photoionization of CA should not have contributed to the degradation of CA in water.

Scheme 1 summarizes the proposed deactivation mechanism of CA (neutral tri-keto) in water, which is based on the calculations reported in this study. It is predicted that excitation at ca. 7.7 eV leads to the population of the $S_{5,6}$ states. Subsequently, following Kasha's rule, [30] the population internally converts to the $S_{1,2}$ states since the possible intersystem crossing pathways from higher lying singlet states are not expected to play a major role in the deactivation of CA due to the negligible magnitude of their spin–orbit couplings. Following internal conversion from the high energy singlet states to the $S_{1,2}$ states, internal conversion to the S_0 state should occur, while intersystem crossing to the T_5 or $T_{1,2}$ states participate to a very minor extent. Considering that the spin–orbit couplings of CA are of the same order of magnitude as those reported for TAP, [31] which is photostable, [6] and that a conical intersection between the S_1 and S_0 can be accessed in a nearly barrierless fashion, it is expected that internal conversion to the ground-state should play a major role in the deactivation of CA, while intersystem crossing to the triplet manifold should not. Collectively, the absorption spectrum shown in Figure 2, the vertical excitation energies reported in Table 1, the spin–orbit couplings reported in Table 2, and the potential energy surface profiles reported in Figure 4, provide compelling computational evidence for the high photostability of CA (tri-keto neutral form) in water under prebiotic conditions, and thus increase the probability of its prospective availability during the prebiotic era.

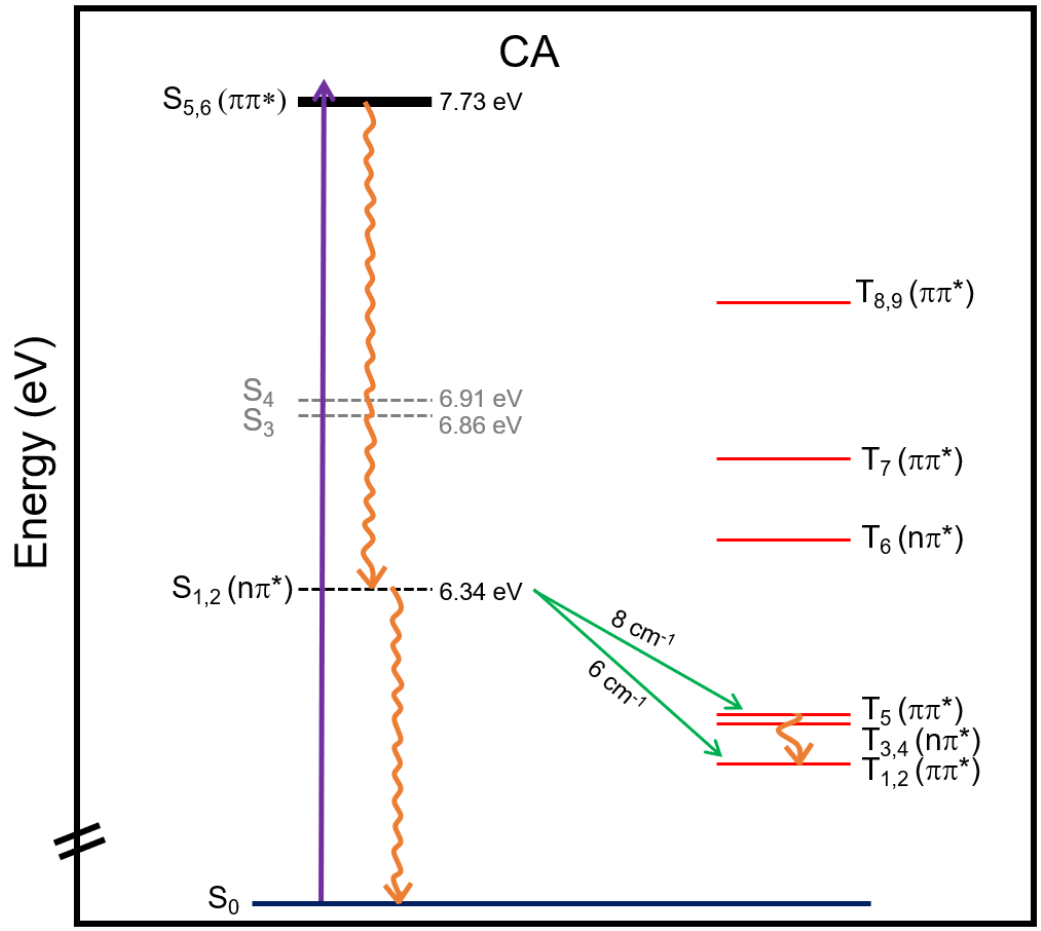

Scheme 1. Proposed deactivation mechanism of CA in water based on the electronic-structure calculations reported in this work. Excitation of CA with ca. 7.7 eV, is predicted to result in ultrafast internal conversion from the $S_{5,6}$ states to the $S_{1,2}$ states and then from the $S_{1,2}$ states to the S_0 state via a C-puckering $(S_1/S_0)_{CI}$ as the primary relaxation mechanism. Intersystem crossing from the $S_{1,2}$ states to the T_5 and/or $T_{1,2}$ state may occur as a very minor pathway in water.

3. Computational Methods

All electronic-structure calculations were performed in ORCA 5.0.0 [45]. All optimizations were performed with the X3LYP functional [20]. The cc-pVDZ [46] basis set was used in all the optimizations. The conductor-like polarizable continuum model (C-PCM) [47] was used to implicitly model bulk solvation. To model solvent effects explicitly, three water molecules were added to form hydrogen bonds with the hydrogen and oxygen atoms. To increase the efficiency of the calculations, the RIJCOSX density fitting approximation was employed [48] This density fitting approximation decomposed the usual four-centered two-electron integrals into three-centered integrals using the corresponding auxiliary basis set. The energy of the radical cation to calculate the vertical ionization energy was obtained by performing a single-point calculation at the UX3LYP/C-PCM/cc-pVDZ level of theory in water, using a charge of +1 and a multiplicity of 2 on the optimized ground-state geometry. The vertical ionization energy was then obtained by subtracting the energy of the ground-state form that of the radical cation.

Vertical excitation energies for relevant singlet and triplet states from the optimized ground state geometry were calculated using the CAM-B3LYP [22] functional and the def2-TZVP basis set [49]. Assignment of the respective character of the excited states was done by considering the oscillator strengths of the states and by visual inspection of the Kohn–Sham orbitals. Spin–orbit coupling matrix elements were computed using the Franck–Condon geometry at the TD-CAM-B3LYP/C-PCM/ def2-TZVP in water. The

geometry of the lowest-energy singlet state was optimized at the TD-X3LYP/C-PCM/cc-pVDZ level of theory in water. The conical intersection between the lowest-energy singlet state and the ground state was optimized using LR-TD-DFT and SF-TD-DFT at the TD-X3LYP/C-PCM/cc-pVDZ in water. To estimate the energy barrier to access the conical intersection calculated with LR-TD-DFT, optimizations along the O6C6N1C2 dihedral angle going from the S_1 minimum-geometry to the $(S_1/S_0)_{CI}$ were performed. To estimate the energy barrier to access the conical intersection calculated with SF-TD-DFT, a minimum-energy path calculation between the S_1 minimum-geometry to the $(S_1/S_0)_{CI}$ was performed at the TD-X3LYP/C-PCM/cc-pVDZ in water using the Nudged Elastic Band method as implemented in ORCA 5.0.0 [50]. The choice to use the minimum energy path calculation over optimizations along the O6C6N1C2 dihedral angle to get the energy barrier to access the $(S_1/S_0)_{CI}$ was made because this calculation was less computationally expensive for the SF-TD-DFT approach. All molecular structures reported in this work were visualized with Avogadro. [51]

4. Conclusions

In this study, DFT and TD-DFT were used to evaluate the likelihood of the photostability of cyanuric acid in water. The calculations suggest that cyanuric acid should be photostable. Specifically, it is shown that the magnitude of the spin–orbit couplings between singlet and triplet states are small, which suggests that intersystem crossing should not play a major role in the deactivation of cyanuric acid. It is also shown that the lowest-energy excited singlet state of cyanuric acid can access a conical intersection with the ground state in a nearly barrierless (≤0.13 eV) fashion. Moreover, we show that photoionization of cyanuric acid is unlikely considering the high vertical ionization energy (8.2 eV) and the electromagnetic radiation that was available in the prebiotic era on the Earth's surface. Therefore, these results provide compelling computational evidence that lends support to the idea that cyanuric acid could have accumulated in large quantities during the prebiotic era, which thus strengthens its candidature as a prebiotic nucleobase.

Supplementary Materials: The following supporting information can be downloaded. Table S1. Vertical excitation energies of microsolvated cyanuric acid (CA) calculated for the first six excited singlet states at the TD-X/CPCM/def2-TZVP in water, where X is the functional used. Oscillator strengths are shown in parentheses [23,24,26,27]; Table S2. Vertical excitation energies for the lowest twelve singlet and twelve triplet states of microsolvated CA calculated at the TD-PBE0/C-PCM/def2-TZVP//X3LYP/C-PCM/cc-pVDZ level of theory in water [28,29]. Table S3. Energy gaps between the calculated excited singlet and triplet states and their corresponding spin-orbit couplings obtained for microsolvated CA at the TD-PBE0/C-PCM/def2-TZVP//X3LYP/C-PCM/cc-pVDZ in water.

Author Contributions: Investigation, formal analysis, writing—original draft, review, and editing, L.A.O.-R.; Writing—original draft, review, and editing, S.J.H.; Conceptualization, funding, acquisition, project administration, resources, supervision, visualiza-tion, validation, writing—review and editing, C.E.C.-H. All authors have read and agreed to the published version of the manuscript.

Funding:

Institutional Review Board Statement:

Informed Consent Statement:

Data Availability Statement:

Acknowledgments: The authors acknowledge funding from the National Science Foundation (Grant No. CHE-1800052). L.A.O.-R. also acknowledges the NSF-AGEP and the NOA-AGEP programs for support. This work made use of the High-Performance Computing Resource in the Core Facility for Advanced Research Computing at Case Western Reserve University. C.E.C.-H. thanks N.V. Hud for bringing the research question explored in this study to his attention.

Conflicts of Interest: The authors declare no conflict of interest.

Sample Availability: Samples of the compounds are available from the authors.

References

1. Hayatsu, R.; Studier, M.H.; Matsuoka, S.; Anders, E. Origin of organic matter in early solar system—VI. Catalytic synthesis of nitriles, nitrogen bases and porphyrin-like pigments. *Geochim. Cosmochim. Acta* **1972**, *36*, 555–571.
2. Hayatsu, R.; Studier, M.H.; Moore, L.P.; Anders, E. Purines and triazines in the Murchison meteorite. *Geochim. Cosmochim. Acta* **1975**, *39*, 471–488.
3. Schaber, P.M.; Colson, J.; Higgins, S.; Thielen, D.; Anspach, B.; Brauer, J. Thermal decomposition (pyrolysis) of urea in an open reaction vessel. *Thermochim. Acta* **2004**, *424*, 131–142.
4. Hayatsu, R.; Studier, M.H.; Oda, A.; Fuse, K.; Anders, E. Origin of organic matter in early solar system—II. Nitrogen compounds. *Geochim. Cosmochim. Acta* **1968**, *32*, 175–190.
5. Jeilani, Y.A.; Orlando, T.M.; Pope, A.; Pirim, C.; Nguyen, M.T. Prebiotic synthesis of triazines from urea: A theoretical study of free radical routes to melamine, ammeline, ammelide and cyanuric acid. *RSC Adv.* **2014**, *4*, 32375–32382.
6. Brister, M.M.; Pollum, M.; Crespo-Hernández, C.E. Photochemical etiology of promising ancestors of the RNA nucleobases. *Phys. Chem. Chem. Phys.* **2016**, *18*, 20097–20103.
7. Cafferty, B.J.; Hud, N.V. Was a Pyrimidine-Pyrimidine Base Pair the Ancestor of Watson-Crick Base Pairs? Insights from a Systematic Approach to the Origin of RNA. *Isr. J. Chem.* **2015**, *55*, 891–905.
8. Seto, C.; Whitesides, G. Self-Assembly Based on the Cyanuric Acid-Melamine Lattice1. *J. Am. Chem. Soc.* **1990**, *112*, 6409–6411.
9. Cafferty, B.J.; Gállego, I.; Chen, M.C.; Farley, K.I.; Eritja, R.; Hud, N.V. Efficient self-assembly in water of long noncovalent polymers by nucleobase analogues. *J. Am. Chem. Soc.* **2013**, *135*, 2447–2450.
10. Chen, M.C.; Cafferty, B.J.; Mamajanov, I.; Gállego, I.; Khanam, J.; Krishnamurthy, R.; Hud, N.V. Spontaneous prebiotic formation of a β-ribofuranoside that self-assembles with a complementary heterocycle. *J. Am. Chem. Soc.* **2014**, *136*, 5640–5646.
11. Karunakaran, S.C.; Cafferty, B.J.; Weigert-Muñoz, A.; Schuster, G.B.; Hud, N.V. Spontaneous Symmetry Breaking in the Formation of Supramolecular Polymers: Implications for the Origin of Biological Homochirality. *Angew. Chem. Int. Ed.* **2019**, *58*, 1453–1457.
12. Sagan, C. Ultraviolet selection pressure on the earliest organisms. *J. Theor. Biol.* **1973**, *39*, 195–200.
13. Ranjan, S.; Sasselov, D.D. Influence of the UV Environment on the Synthesis of Prebiotic Molecules. *Astrobiology* **2016**, *16*, 68–88.
14. Ranjan, S.; Sasselov, D.D. Constraints on the Early Terrestrial Surface UV Environment Relevant to Prebiotic Chemistry. *Astrobiology* **2017**, *17*, 169–204.
15. Dodd, M.S.; Papineau, D.; Grenne, T.; Slack, J.F.; Rittner, M.; Pirajno, F.; O'Neil, J.; Little, C.T.S. Evidence for early life in Earth's oldest hydrothermal vent precipitates. *Nature* **2017**, *543*, 60–64.
16. Cavalazzi, B.; Lemelle, L.; Simionovici, A.; Cady, S.L.; Russell, M.J.; Bailo, E.; Canteri, R.; Enrico, E.; Manceau, A.; Maris, A.; et al. Cellular remains in a ~3.42-billion-year-old subseafloor hydrothermal environment. *Sci. Adv.* **2021**, *7*, 1–9.
17. Betts, H.C.; Puttick, M.N.; Clark, J.W.; Williams, T.A.; Donoghue, P.C.J.; Pisani, D. Integrated genomic and fossil evidence illuminates life's early evolution and eukaryote origin. *Nat. Ecol. Evol.* **2018**, *2*, 1556–1562.
18. Krissansen-Totton, J.; Arney, G.N.; Catling, D.C. Constraining the climate and ocean pH of the early Earth with a geological carbon cycle model. *Proc. Natl. Acad. Sci. USA* **2018**, *115*, 4105–4110.
19. Sancier, K.M.; Brady, A.P.; Lee, W.W. Absorption spectra of solutions of cyanuric acid and its chlorinated derivatives. *Spectrochim. Acta* **1964**, *20*, 397–403.
20. Xu, X.; Goddard, W.A. The X3LYP extended density functional for accurate descriptions of nonbond interactions, spin states, and thermochemical properties. *Proc. Natl. Acad. Sci. USA* **2004**, *101*, 2673–2677.
21. Rao, L.; Ke, H.; Fu, G.; Xu, X.; Yan, Y. Performance of several density functional theory methods on describing hydrogen-bond interactions. *J. Chem. Theory Comput.* **2009**, *5*, 86–96.
22. Yanai, T.; Tew, D.P.; Handy, N.C. A new hybrid exchange--correlation functional using the Coulomb-attenuating method (CAM-B3LYP). *Chem. Phys. Lett.* **2004**, *393*, 51–57.
23. Chai, J.D.; Head-Gordon, M. Systematic optimization of long-range corrected hybrid density functionals. *J. Chem. Phys.* **2008**, *128*, 84106.
24. Iikura, H.; Tsuneda, T.; Yanai, T.; Hirao, K. A long-range correction scheme for generalized-gradient-approximation exchange functionals. *J. Chem. Phys.* **2001**, *115*, 3540–3544.
25. Adamo, C.; Barone, V. Toward reliable density functional methods without adjustable parameters: The PBE0 model. *J. Chem. Phys.* **1999**, *110*, 6158–6170.
26. Silva-Junior, M.R.; Schreiber, M.; Sauer, S.P.A.; Thiel, W. Benchmarks for electronically excited states: Time-dependent density functional theory and density functional theory based multireference configuration interaction. *J. Chem. Phys.* **2008**, *129*, 104103.
27. Winter, N.O.C.; Graf, N.K.; Leutwyler, S.; Hättig, C. Benchmarks for 0--0 transitions of aromatic organic molecules: DFT/B3LYP, ADC (2), CC2, SOS-CC2 and SCS-CC2 compared to high-resolution gas-phase data. *Phys. Chem. Chem. Phys.* **2013**, *15*, 6623–6630.
28. El-Sayed, M.A. The triplet state: Its radiative and nonradiative properties. *Acc. Chem. Res.* **1968**, *1*, 8–16.
29. El-Sayed, M.A. Spin-orbit coupling and the radiationless processes in nitrogen heterocyclics. *J. Chem. Phys.* **1963**, *38*, 2834–2838.

30. Kasha, M. Characterization of electronic transitions in complex molecules. *Discuss. Faraday Soc.* **1950**, *9*, 14–19.
31. Rankine, C.D. Ultrafast excited-state dynamics of promising nucleobase ancestor 2, 4, 6-triaminopyrimidine. *Phys. Chem. Chem. Phys.* **2021**, *23*, 4007–4017.
32. Serrano-Andres, L.; Merchán, M. Are the five natural DNA/RNA base monomers a good choice from natural selection? A photochemical perspective. *J. Photochem. Photobiol. C Photochem. Rev.* **2009**, *10*, 21–32.
33. Giussani, A.; Serra-Martí, J.; Roca-Sanjuán, D.; Merchán, M. Excitation of Nucleobases from a Computational Perspective I: Reaction Paths. *Top. Curr. Chem.* **2015**, *355*, 57–98.
34. Pepino, A.J.; Segarra-Martí, J.; Nenov, A.; Improta, R.; Garavelli, M. Resolving ultrafast photoinduced deactivation in water-solvated pyrimidines nucleosides. *J. Phys. Chem. Lett.* **2017**, *8*, 1777–1783.
35. Brister, M.M.; Crespo-Hernández, C.E. Excited-state dynamics in the RNA nucleotide uridine 5′-monophosphate investigated using femtosecond broadband transient absorption spectroscopy. *J. Phys. Chem. Lett.* **2019**, *10*, 2156–2161.
36. Hoehn, S.J.; Krul, S. Crespo-Hernández, Increased Photostability of the Integral mRNA Vaccine Component N1-Methylpseudouridine Compared to Uridine. *Chem. A Eur. J.* **2021**, *28*, e202103667. https://doi.org/10.1002/chem.202103667.
37. Hoehn, S.J.; Caldero-Rodríguez, N.E.; Crespo-Hernández, C.E. Photochemistry of RNA, RNA Monomers and their Plausible Prebiotic Precursors. *Photochem. Photobiol. Sci.* **2021**, *9*, 197–226.
38. Pollum, M.; Martinez-Fernandez, L.; Crespo-Hernandez, C.E. Photochemistry of nucleic acid bases and their thio- and aza-analogues in solution. *Top. Curr. Chem.* **2015**, *47*, 245–327.
39. Matsika, S. Electronic Structure Methods for the Description of Nonadiabatic Effects and Conical Intersections. *Chem. Rev.* **2021**, *121*, 9407–9449.
40. Krylov, A.I. Size-consistent wave functions for bond-breaking: The equation-of-motion spin-flip model. *Chem. Phys. Lett.* **2001**, *338*, 375–384.
41. Krylov, A.I. Spin-flip equation-of-motion coupled-cluster electronic structure method for a description of excited states, bond breaking, diradicals, and triradicals. *Acc. Chem. Res*. **2006**, *39*, 83–91.
42. Slipchenko, L.V.; Krylov, A.I. Singlet-triplet gaps in diradicals by the spin-flip approach: A benchmark study. *J. Chem. Phys*. **2002**, *117*, 4694–4708.
43. Huix-Rotllant, M.; Natarajan, B.; Ipatov, A.; Wawire, C.M.; Deutsch, T.; Casida, M.E. Assessment of noncollinear spin-flip Tamm-Dancoff approximation time-dependent density-functional theory for the photochemical ring-opening of oxirane. *Phys. Chem. Chem. Phys*. **2010**, *12*, 12811–12825.
44. Minezawa, N.; Gordon, M.S. Optimizing conical intersections by spin- flip density functional theory: Application to ethylene. *J. Phys. Chem. A* **2009**, *113*, 12749–12753.
45. Neese, F.; Wennmohs, F.; Becker, U.; Riplinger, C. The ORCA quantum chemistry program package. *J. Chem. Phys.* **2020**, *152*, 224108.
46. Dunning, T.H., Jr. Gaussian basis sets for use in correlated molecular calculations. I. The atoms boron through neon and hydrogen. *J. Chem. Phys.* **1989**, *90*, 1007–1023.
47. Barone, V.; Cossi, M. Quantum calculation of molecular energies and energy gradients in solution by a conductor solvent model. *J. Phys. Chem. A* **1998**, *102*, 1995–2001.
48. Neese, F.; Wennmohs, F.; Hansen, A.; Becker, U. Efficient, approximate and parallel Hartree--Fock and hybrid DFT calculations. A 'chain-of-spheres' algorithm for the Hartree-Fock exchange. *Chem. Phys.* **2009**, *356*, 98–109.
49. Weigend, F.; Ahlrichs, R. Balanced basis sets of split valence, triple zeta valence ad quadruple zeta valence quality for H to Rn: Design and assessment of accuracy. *Phys. Chem. Chem. Phys.* **2005**, *7*, 3297–3305.
50. Ásgeirsson, V.; Birgisson, B.O.; Bjornsson, R.; Becker, U.; Neese, F.; Riplinger, C.; Jónsson, H. Nudged elastic band method for molecular reactions using energy-weighted springs combined with eigenvector following. *J. Chem. Theory Comput.* **2021**, *17*, 4929–4945.
51. Hanwell, M.D.; Curtis, D.E.; Lonie, D.C.; Vandermeersch, T.; Zurek, E.; Hutchison, G.R. Avogadro: An advanced semantic chemical editor, visualization, and analysis platform. *J. Cheminform.* **2012**, *4*, 1–17.